Daniel Laidig*, Philipp Müller and Thomas Seel

Automatic anatomical calibration for IMU-based elbow angle measurement in disturbed magnetic fields

Abstract: Inertial Measurement Units (IMUs) are increasingly used for human motion analysis. However, two major challenges remain: First, one must know precisely in which orientation the sensor is attached to the respective body segment. This is commonly achieved by accurate manual placement of the sensors or by letting the subject perform tedious calibration movements. Second, standard methods for inertial motion analysis rely on a homogeneous magnetic field, which is rarely found in indoor environments. To address both challenges, we introduce an automatic calibration method for joints with two degrees of freedom such as the combined radioulnar and elbow joint. While the user performs arbitrary movements, the method automatically identifies the sensor-to-segment orientations by exploiting the kinematic constraints of the joint. Simultaneously, the method identifies and compensates the influence of magnetic disturbances on the sensor orientation quaternions and the joint angles. In experimental trials, we obtain angles that agree well with reference values from optical motion capture. We conclude that the proposed method overcomes mounting and calibration restrictions and improves measurement accuracy in indoor environments. It therefore improves the practical usability of IMUs for many medical applications.

Keywords: Automatic anatomical calibration, sensor-to-segment calibration, elbow joint, kinematic constraints.

https://doi.org/10.1515/cdbme-2017-0035

1 Introduction

While marker-based optical motion capture is considered a gold standard for human motion analysis, this method is confined to expensive laboratory environments. In contrast, Inertial Measurement Units (IMUs) facilitate ambulatory realtime motion analysis with comparably good accuracy, see e.g. [4-6]. However, the orientation of each IMU with respect to its body segment must be known to derive useful kinematic quantities. This is commonly achieved by accurate manual placement of the IMUs [1] or by asking the subject to perform tedious calibration movements [3]. However, it was recently demonstrated that sensor-to-segment orientations can also be determined from the data of arbitrary upper or lower limb motions [4, 6]. This is achieved by exploiting the kinematic constraints imposed by the approximate 1D joint (knee) or 2D joint (combined radioulnar and elbow joint). These methods highly increase the practical usability of IMUs in clinical applications. However, as the vast majority of IMU-based motion analysis protocols, the method for 2D joints relies on a homogeneous magnetic field, which is

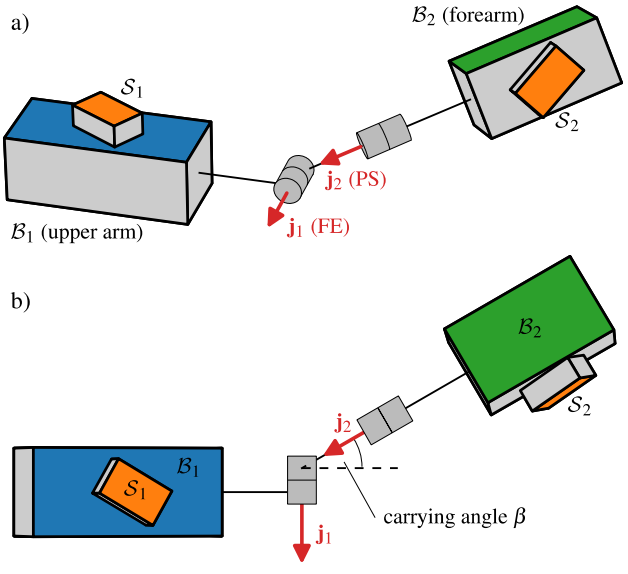

Figure 1: *(a)* Kinematic model of the elbow joint. Upper arm and forearm are connected by two revolute joints, allowing for flexion/extension and pronation/supination. The goal of anatomical calibration is to determine $\mathbf{j}_1$ and $\mathbf{j}_2$ in the frame of the respective IMU. *(b)* View onto the $\mathbf{j}_1$-$\mathbf{j}_2$ plane. The carrying angle is described by a fixed rotation between flexion/extension and pronation/supination, as recommended by [9].

***Corresponding author: Daniel Laidig:** Control Systems Group, TU Berlin, Germany, e-mail: laidig@control.tu-berlin.de
Philipp Müller, Thomas Seel: Control Systems Group, TU Berlin, Germany, e-mail: {mueller,seel}@control.tu-berlin.de

Open Access. © 2017 Daniel Laidig et al., published by De Gruyter. This work is licensed under the Creative Commons Attribution-NonCommercial-NoDerivatives 4.0 License.

Brought to you by | Technische Universität Berlin
Authenticated
Download Date | 12/13/17 2:46 PM

rarely found in indoor environments. This implies that magnetic disturbances cannot only affect the measured joint angles, but can also decrease the accuracy of the automatic anatomical calibration. In the current contribution, we build upon the previous work [4] and propose a method for automatic sensor-to-segment calibration that identifies and compensates the effect of magnetic disturbances.

We model the joint rotation using Euler angles, as recommended in [9]. The rotation sequence consists of flexion/extension, a fixed carrying angle, and pronation/supination, cf. Fig. 1. This implies that the flexion/extension (FE) axis $\mathbf{j}_1$ is fixed in the upper arm frame, while the pronation/supination (PS) axis $\mathbf{j}_2$ is fixed in the forearm frame. The goal of anatomical calibration is to determine the (constant) coordinates $\mathbf{j}_1$ and $\mathbf{j}_2$ in the local coordinate systems of the upper arm sensor and forearm sensor, respectively.

2 Method

Two inertial sensors $\mathcal{S}_1$ and $\mathcal{S}_2$ are placed on the subject's upper arm and forearm in unknown orientations and measure the angular rates $\boldsymbol{\omega}_1(t)$ and $\boldsymbol{\omega}_2(t)$ in local coordinates. We use (potentially on-chip) sensor fusion of the gyroscope, accelerometer and magnetometer readings to obtain estimates of the quaternions ${}^{\mathcal{S}1}_{\mathcal{E}}\mathbf{q}$ and ${}^{\mathcal{S}2}_{\mathcal{E}}\mathbf{q}$ describing the sensor orientation w.r.t. a fixed frame $\mathcal{E}$. To this end, we use a recent sensor fusion algorithm that limits the influence of magnetic disturbances to the heading while keeping the inclination unaffected [7]. The effect of magnetic disturbances can therefore be expressed by the estimated orientations ${}^{\mathcal{S}1}_{\mathcal{E}1}\mathbf{q}$ and ${}^{\mathcal{S}2}_{\mathcal{E}2}\mathbf{q}$ being given in different global reference frames $\mathcal{E}_1$ and $\mathcal{E}_2$, which are rotated around the vertical global z-axis (cf. [2]), i.e.

$$ {}^{\mathcal{E}2}_{\mathcal{E}1}\mathbf{q} = \left[\cos\left(\frac{\delta}{2}\right) \quad 0 \quad 0 \quad \sin\left(\frac{\delta}{2}\right)\right]^{\mathrm{T}} \tag{1} $$

with $\delta(t)$ being the heading error that is caused by the magnetic disturbance.

We introduce the square bracket operator to express when a three-dimensional vector is transformed into another coordinate system by multiplying it with the respective quaternion and its inverse, e.g.

$$ [\mathbf{j}_1]_{\mathcal{E}} = {}^{\mathcal{S}1}_{\mathcal{E}}\mathbf{q} \otimes \mathbf{j}_1 \otimes {}^{\mathcal{S}1}_{\mathcal{E}}\mathbf{q}^{-1}. \tag{2} $$

2.1 Joint constraint in angular rates

The addition theorem for angular velocities allows us to express the relationship between $\boldsymbol{\omega}_1(t)$ and $\boldsymbol{\omega}_2(t)$ as

$$ [\boldsymbol{\omega}_2]_{\mathcal{E}} = [\boldsymbol{\omega}_1]_{\mathcal{E}} + \omega_{\mathrm{j}1}[\mathbf{j}_1]_{\mathcal{E}} + \omega_{\mathrm{j}2}[\mathbf{j}_2]_{\mathcal{E}}, \tag{3} $$

with $\omega_{\mathrm{j}1}$ being the scalar FE angular rate and $\omega_{\mathrm{j}2}$ being the scalar PS angular rate.[1] We assume a heading error $\delta(t) \neq 0$ and thus replace $\mathcal{E}$ by $\mathcal{E}_1$. Taking the scalar product with $[\mathbf{j}_1]_{\mathcal{E}1} \times [\mathbf{j}_2]_{\mathcal{E}1}$ on both sides and making use of the fact that $\mathbf{a} \cdot (\mathbf{a} \times \mathbf{b}) = \mathbf{a} \cdot (\mathbf{b} \times \mathbf{a}) = 0$ yields

$$ \Big(\underbrace{[\boldsymbol{\omega}_1]_{\mathcal{E}1} - [\boldsymbol{\omega}_2]_{\mathcal{E}1}}_{=:\boldsymbol{\omega}_{\mathrm{rel}}}\Big) \cdot \underbrace{([\mathbf{j}_1]_{\mathcal{E}1} \times [\mathbf{j}_2]_{\mathcal{E}1})}_{=:\mathbf{j}_{\mathrm{n}}} = 0. \tag{4} $$

This constraint must be fulfilled for each sampling instant and can therefore be used to estimate the joint axes from a large number of data sets $\{\boldsymbol{\omega}_1(t), \boldsymbol{\omega}_2(t), {}^{\mathcal{S}1}_{\mathcal{E}1}\mathbf{q}(t), {}^{\mathcal{S}2}_{\mathcal{E}1}\mathbf{q}(t)\}$.

To evaluate the joint constraint, we need the quaternions ${}^{\mathcal{S}1}_{\mathcal{E}1}\mathbf{q}$ and ${}^{\mathcal{S}2}_{\mathcal{E}1}\mathbf{q} = {}^{\mathcal{E}2}_{\mathcal{E}1}\mathbf{q} \otimes {}^{\mathcal{S}2}_{\mathcal{E}2}\mathbf{q}$. Calculating the latter requires knowing the heading error $\delta(t)$. Assume that, on short time scales, the heading error is constant or almost linear in time, i.e. it can be approximated by

$$ \delta(t) \approx at + b, \qquad a, b \in \mathbb{R}. \tag{5} $$

This means that during the automatic sensor-to-segment calibration, both the joint axis coordinates and the heading difference (i.e. a and b) must be identified.

2.2 Joint axes parametrization

The joint axes $\mathbf{j}_1 \in \mathbb{R}^3$ and $\mathbf{j}_2 \in \mathbb{R}^3$ are unit vectors and can be expressed using the spherical coordinates

$$ \mathbf{j}_i = [\sin\theta_i \cos\varphi_i \quad \sin\theta_i \sin\varphi_i \quad \cos\theta_i]^{\mathrm{T}}, \; i = 1, 2, \tag{6} $$

or the alternative spherical representation

$$ \mathbf{j}_i = [\cos\theta_i \quad \sin\theta_i \sin\varphi_i \quad \sin\theta_i \cos\varphi_i]^{\mathrm{T}}, \; i = 1, 2. \tag{7} $$

To avoid the singularity $\partial\mathbf{j}_i/\partial\varphi_i = 0$, we switch from one representation to the other whenever $|\sin\theta_i| < 0.5$.

2.3 Cost function and optimization

With the parameter vector $\boldsymbol{\Phi} := [\theta_1 \; \varphi_1 \; \theta_2 \; \varphi_2 \; a \; b]^{\mathrm{T}}$ we define the error for each sampling instant k as

$$ e(\boldsymbol{\Phi})_k := \boldsymbol{\omega}_{\mathrm{rel}}(a, b) \cdot \mathbf{j}_{\mathrm{n}}(\boldsymbol{\Phi}). \tag{8} $$

Making use of the fact that the product rule holds for quaternion multiplication and by using Rodrigues' rotation formula, we calculate analytical expressions for the gradient $\mathrm{d}e/\mathrm{d}\boldsymbol{\Phi}$ that only depend on the parameters $\boldsymbol{\Phi}$ and on the measurements $\boldsymbol{\omega}_1$, $\boldsymbol{\omega}_2$, ${}^{\mathcal{S}1}_{\mathcal{E}1}\mathbf{q}$ and ${}^{\mathcal{S}2}_{\mathcal{E}2}\mathbf{q}$.

For a set of N measurement samples and a given

1 Note that the carrying angle does not appear, since it is time-invariant and all quantities are expressed in global coordinates.

Brought to you by | Technische Universität Berlin
Authenticated
Download Date | 12/13/17 2:46 PM

parameter vector, we can therefore calculate the error vector $\mathbf{e} \coloneqq [e_1\ e_2\ \dots\ e_N]^{\mathrm{T}}$ and the Jacobian $\mathbf{J} \in \mathbb{R}^{N\times 6}$ with

$$[\mathbf{J}]_{ij} = \frac{\partial e_i}{\partial \Phi_j}. \tag{9}$$

To estimate the joint axes $\mathbf{j}_1$ and $\mathbf{j}_2$ and the heading difference $\delta(t) = at + b$, we minimize the sum of squares $\mathbf{e}^{\mathrm{T}}\mathbf{e}$ using the Gauss-Newton algorithm [8].

2.4 Magnetic disturbance compensation

Having identified a, b, we compensate the influence of magnetic disturbances on the estimated orientations by calculating ${}^{\mathcal{E}2}_{\mathcal{E}1}\mathbf{q}$ via (1) and transforming ${}^{\mathcal{S}2}_{\mathcal{E}2}\mathbf{q}$ to $\mathcal{E}_1$, i.e. ${}^{\mathcal{S}2}_{\mathcal{E}1}\mathbf{q} = {}^{\mathcal{E}2}_{\mathcal{E}1}\mathbf{q} \otimes {}^{\mathcal{S}2}_{\mathcal{E}2}\mathbf{q}$, or vice versa. Thereby, we assure that the relative orientation ${}^{\mathcal{S}2}_{\mathcal{S}1}\mathbf{q} = {}^{\mathcal{S}1}_{\mathcal{E}1}\mathbf{q}^{-1} \otimes {}^{\mathcal{S}2}_{\mathcal{E}1}\mathbf{q}$ of both sensors is not affected by the magnetic disturbance.

Note that the linear approximation of the heading difference will only be valid for short time windows. However, once the joint axis coordinates are identified, we can keep them fixed and solve the least-squares problem repeatedly for a and b only. Thereby, we can track the heading difference and compensate its influence on the relative orientation of the sensors repeatedly.

2.5 Joint angle calculation

As a result of the automatic sensor-to-segment calibration and the magnetic disturbance compensation, we know the joint axes $\mathbf{j}_1$ and $\mathbf{j}_2$ in local sensor coordinates and the orientation estimates ${}^{\mathcal{S}1}_{\mathcal{E}1}\mathbf{q}$ and ${}^{\mathcal{S}2}_{\mathcal{E}1}\mathbf{q}$ in a common reference frame. In order to calculate meaningful joint angles, i.e. Euler angles of the relative orientation of one segment with respect to the other, we must calculate body segment orientations from the sensor orientations. With the axis-angle representation of quaternions

$$(\alpha, \mathbf{u}) \coloneqq \begin{bmatrix} \cos\left(\frac{\alpha}{2}\right) \\ \sin\left(\frac{\alpha}{2}\right)\mathbf{u}/\|\mathbf{u}\| \end{bmatrix} \tag{10}$$

we can determine segment-to-sensor orientations

$${}^{\mathcal{B}1'}_{\mathcal{S}1}\mathbf{q} = (\arccos([0\ 0\ 1]^{\mathrm{T}} \cdot \mathbf{j_1}), [0\ 0\ 1]^{\mathrm{T}} \times \mathbf{j_1}) \tag{11}$$

$${}^{\mathcal{B}2'}_{\mathcal{S}2}\mathbf{q} = (\arccos([0\ 1\ 0]^{\mathrm{T}} \cdot \mathbf{j_2}), [0\ 1\ 0]^{\mathrm{T}} \times \mathbf{j_2}) \tag{12}$$

that ensure that the respective joint axes correspond to the axes defined by the ISB [9]. This allows us to calculate the relative segment orientation

$${}^{\mathcal{B}2'}_{\mathcal{B}1'}\mathbf{q} = \left({}^{\mathcal{S}1}_{\mathcal{E}1}\mathbf{q} \otimes {}^{\mathcal{B}1'}_{\mathcal{S}1}\mathbf{q}\right)^{-1} \otimes {}^{\mathcal{S}2}_{\mathcal{E}1}\mathbf{q} \otimes {}^{\mathcal{B}2'}_{\mathcal{S}2}\mathbf{q}. \tag{13}$$

Calculating z-x'-y'' Euler angles $(\alpha', \beta', \gamma')$ of ${}^{\mathcal{B}2'}_{\mathcal{B}1'}\mathbf{q}$ yields the FE angle α', the (ideally fixed) carrying angle β', and the PS angle γ'. However, α' and γ' still have an unknown zero point that depends on the actual sensor placement.[2] To determine this zero point, assume that the true joint angles α_{r} and γ_{r} at $t = t_{\mathrm{r}}$ are known. Evaluating ${}^{\mathcal{B}2'}_{\mathcal{B}1'}\mathbf{q}$ at $t = t_{\mathrm{r}}$, we obtain α_{o} and γ_{o} and calculate

$${}^{\mathcal{B}1}_{\mathcal{S}1}\mathbf{q} = {}^{\mathcal{B}1'}_{\mathcal{S}1}\mathbf{q} \otimes (\alpha_{\mathrm{o}} - \alpha_{\mathrm{r}}, [0\ 0\ 1]^{\mathrm{T}}), \tag{14}$$

$${}^{\mathcal{B}2}_{\mathcal{S}2}\mathbf{q} = {}^{\mathcal{B}2'}_{\mathcal{S}2}\mathbf{q} \otimes (\gamma_{\mathrm{r}} - \gamma_{\mathrm{o}}, [0\ 1\ 0]^{\mathrm{T}}), \tag{15}$$

which yields the relative orientation ${}^{\mathcal{B}2}_{\mathcal{B}1}\mathbf{q}$ and the joint angles (α, β, γ) with the desired values at $t = t_{\mathrm{r}}$.

3 Experimental validation

We validate the proposed method against an optical motion capture system (Vicon Motion Systems Ltd. UK). Optical markers are placed on bony landmarks that allow for the measurement of the elbow angles according to the ISB recommendations [9]. Inertial sensors (XSens MTw, Xsens Technologies B.V., Netherlands) are placed on upper arm close to the elbow and on the forearm close to the wrist. The subject performs a sequence of pick-and-place and drinking motions. In total, 12 trials with three different velocities are used, with the trial duration ranging from 7 s to 17 s. To simulate a worst-case scenario, we add an additional heading disturbance with an amplitude of 80° to the magnetic field measurements.

The proposed joint axis estimation, magnetic disturbance compensation and joint angle calculation method is applied for each trial. We compare the resulting angles to the angles obtained from the optical reference system. At the first time instant of each trial, we use the optical angles to determine $\alpha_{\mathrm{o}} - \alpha_{\mathrm{r}}$ and $\gamma_{\mathrm{r}} - \gamma_{\mathrm{o}}$ as described in Section 2.5.

Figure 2 shows inertial and optical angles for an exemplary trial. Note that the angles agree well despite the large heading disturbance that was added to the measurement data. Note furthermore that the deviation between both angles is not zero-mean but instead consists of a constant offset and a time-varying component. Table 1 presents results from all analyzed trials. On average, we obtain flexion/extension and pronation/supination angles with offsets of 4.1° and -5.2° degrees and standard deviations of 3.4° and 6.6°, respectively. The standard deviations are within typical ranges [4] and the offsets might be due to small differences of the zero-pose angles or the identified joint axes.

2 Note e.g. that, for every $\mathbf{j}_2$, there are infinitely many possible orientations in which sensor 2 might be attached to the forearm.

Brought to you by | Technische Universität Berlin
Authenticated
Download Date | 12/13/17 2:46 PM

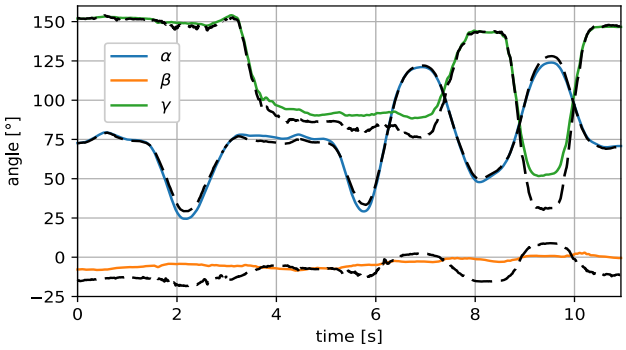

Figure 2: Comparison of the FE angle α, the carrying angle β and the PS angle γ for a representative trial. The IMU-based angles obtained with the proposed method (solid) agree well with the optical reference angles (dashed). Also, note that the IMU-based carrying angle varies less than the reference.

Table 1: Deviations between inertial and optical measurements [°].

Trials	Stand. Dev.		Offset		stdev(β)	
1-12	**FE**	**SP**	**FE**	**SP**	**IMU**	**Opt.**
Min	2.25	4.86	-0.60	-8.13	1.06	6.52
Max	5.74	7.88	8.79	-3.22	3.67	8.22
Mean	**3.43**	**6.63**	**4.09**	**-5.16**	**2.14**	**7.44**
St. Dev.	0.95	0.75	2.95	1.53	0.73	0.49

Table 1 also compares the standard deviation of the carrying angle β for both methods. If the real joint exhibits two degrees of freedom (Fig. 1) and the joint axes are accurately known, then the carrying angle should be constant. Averaged over all trials, the standard deviation of the IMU-based carrying angle is 2.1°, while the standard deviation of the optical reference carrying angle is 7.4°. This suggests that the joint axes found by the proposed method describe the two-degrees-of-freedom joint better than the axes determined by bony landmarks and the optical reference system.

4 Conclusions

We proposed a method for automatic sensor-to-segment (anatomical) calibration that overcomes mounting and calibration restrictions by exploiting the kinematic constraints of joints with two degrees of freedom. Since it compensates the effect of magnetic disturbances, the method is highly suitable for indoor environments. For both reasons, it improves the practical usability of IMUs for many clinical and biomedical applications. Future work will focus on repeated online estimation of the joint axes and the magnetic disturbance.

Author's Statement

Research funding: This work was partially supported by the German Federal Ministry of Education and Research (BMBF) (FKZ16SV7069K). Conflict of interest: Authors state no conflict of interest. Informed consent: Informed consent has been obtained from all individuals included in this study. Ethical approval: The research related to human use complies with all the relevant national regulations, institutional policies and was performed in accordance with the tenets of the Helsinki Declaration, and has been approved by the authors' institutional review board or equivalent committee.

References

[1] A. G. Cutti, A. Giovanardi, L. Rocchi, A. Davalli, and R. Sacchetti. Ambulatory measurement of shoulder and elbow kinematics through inertial and magnetic sensors. Medical & biological engineering & computing, 46(2):169–178, 2008.

[2] D. Laidig, T. Schauer, and T. Seel. Exploiting kinematic constraints to compensate magnetic disturbances when calculating joint angles of approximate hinge joints from orientation estimates of inertial sensors. In Proc. of the 15th IEEE Conf. on Rehabilitation Robotics (accepted), 2017.

[3] H. J. Luinge, P. H. Veltink, and C. T. Baten. Ambulatory measurement of arm orientation. Journal of biomechanics, 40(1):78–85, 2007.

[4] P. Müller, M. A. Begin, T. Schauer, and T. Seel. Alignment-free, self-calibrating elbow angles measurement using inertial sensors. IEEE Journal of Biomedical and Health Informatics, 21(2):312–319, 2017.

[5] T. Seel, D. Graurock, and T. Schauer. Realtime assessment of foot orientation by accelerometers and gyroscopes. Current Directions in Biomedical Engineering, 1(1):466–469, 2015.

[6] T. Seel, J. Raisch, and T. Schauer. IMU-based joint angle measurement for gait analysis. Sensors, 14(4):6891–6909, 2014.

[7] T. Seel and S. Ruppin. Eliminating the effect of magnetic disturbances on the inclination estimates of inertial sensors. In Proc. of 20th IFAC World Congress (to appear in IFACPapersOnLine), 2017.

[8] S. Wright and J. Nocedal. Numerical optimization. Springer Science, 35:67–68, 1999.

[9] G. Wu, F. C. Van der Helm, H. D. Veeger, M. Makhsous, P. Van Roy, C. Anglin, J. Nagels, A. R. Karduna, K. McQuade, X. Wang, et al. ISB recommendation on definitions of joint coordinate systems of various joints for the reporting of human joint motion—part II: shoulder, elbow, wrist and hand. Journal of biomechanics, 38(5):981–992, 2005.

Brought to you by | Technische Universität Berlin
Authenticated
Download Date | 12/13/17 2:46 PM